Urban Forestry & Urban Greening 99 (2024) 128438

Contents lists available at ScienceDirect

Urban Forestry & Urban Greening

journal homepage: www.elsevier.com/locate/ufug

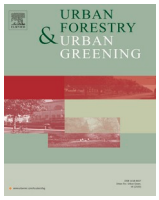

Original article

Exploring how the heterogeneous urban landscape influences CO_2 concentrations: The case study of the Metropolitan Area of Barcelona

Carme Estruch [a], Roger Curcoll [a,c], Josep-Anton Morguí [a,b], Ricard Segura-Barrero [a], Verònica Vidal [a,d], Alba Badia [a], Sergi Ventura [a], Joan Gilabert [a,e], Gara Villalba [a,f,*]

[a] Institute of Environmental Sciences and Technology, Universitat Autònoma de Barcelona (UAB), Bellaterra, Barcelona, Spain
[b] Department of Evolutionary Biology, Ecology and Environmental Science, University of Barcelona, Barcelona, Spain
[c] Institute of Energy Technologies, Universitat Politècnica de Catalunya, Barcelona, Spain
[d] Department of Computer Architecture and Operating Systems, UAB, Bellaterra, Barcelona, Spain
[e] Cartographic and Geological Institute of Catalonia, Parc de Montjuïc, Barcelona, Spain
[f] Department of Chemical, Biological and Environmental Engineering, School of Engineering, UAB, Bellaterra, Barcelona, Spain

ARTICLE INFO

Keywords:
Air density
Urban vegetation
Carbon dioxide
Urban boundary layer
Spatial gradient

ABSTRACT

Monitoring CO_2 concentrations in urban areas is crucial for determining the efficacy of climate change mitigation policies. However, highly heterogeneous land use, local geography, and local convection patterns, which vary throughout the urban landscape, complicate this task. To establish continuous monitoring programs, it is important to first determine the heterogeneity of urban landscapes on the ground. To understand the role these factors play in the distribution of CO_2 over an urban area, we conducted a CO_2 measurement campaign over the Metropolitan Area of Barcelona (AMB) over four urban land uses: impervious, green, forest, and agricultural. There is a clear tendency for CO_2 mixing ratios to decrease as the degree of urban vegetation increases, even in the midst of a developed boundary layer. For example, CO_2 concentrations were 429 and 427 ppm at forest and agricultural sites, respectively, while 485 ppm was reported at urban sites. A decrease in atmospheric CO_2 was observed from 458 to 428 ppm in the gradient from urban to suburban areas, in which the biosphere component increased. The biosphere component of the CO_2 signal was significant and was observed in the gradient from urban to suburban areas, which averaged a reduction from 458 to 428 ppm. Our findings show that the large spatial variability in CO_2 concentrations (ranging from 410 to 495 ppm) is best explained by anthropogenic activity. We propose increasing the spatiotemporal resolution of CO_2 monitoring in the AMB to determine these trends more precisely over longer periods of time.

1. Introduction

Cities are key players in the Paris Agreement to reduce greenhouse gas (GHG) emissions since they emit 70 % of the carbon related to the energy sector (IEA, 2016). Currently, many cities are adopting measures to reduce carbon emissions through various initiatives, such as the Green Deal (European Commission, 2019), the Covenant of Mayors (Covenant of Mayors, 2009) or the C40 (https://www.c40.org/) network. Some of these strategies include increasing urban green infrastructure (McHale et al., 2007), which can provide carbon dioxide (CO_2) uptake (i.e., Zhang et al., 2019), as well as other ecosystem services such as shading, cooling (Rahman et al., 2020), and air pollution removal (Xu et al., 2020). Some studies have shown that the rate of CO_2 uptake by urban biosphere photosynthesis is positively related to the vegetation fraction in urban landscapes (i.e., Bergeron and Strachan, 2011; Villalba et al., 2021). However, these interventions should be accompanied by long-term in situ monitoring of the urban atmosphere gas composition to determine whether and to what extent mitigation strategies are effective over time. These measurements can also serve to validate GHG inventory accounts determined by city administration as well as urban GHG modeling efforts and to create repositories of atmospheric C distribution in cities (i.e., da Silva et al., 2019; Lietzke and Vogt, 2013).

Measurements of CO_2 in urban areas are difficult to interpret and attribute to land-use sources and sinks in great part due to the gas transport provoked by regional and local convection, which is

* Corresponding author at: Institute of Environmental Sciences and Technology, Universitat Autònoma de Barcelona (UAB), Bellaterra, Barcelona, Spain
E-mail address: gara.villalba@uab.cat (G. Villalba).

https://doi.org/10.1016/j.ufug.2024.128438
Received 20 November 2023; Received in revised form 11 May 2024; Accepted 3 July 2024
Available online 13 July 2024

influenced by the heterogeneous nature of the urban landscapes (Briber et al., 2013; Font et al., 2015). The daily cycle of the planetary boundary layer (PBL) is responsible for air mixing and is in turn influenced by thermal mixing, moisture, and terrain roughness. Additionally, underneath the PBL, the urban boundary layer (UBL) (Oke, 1976) is created by the difference in mixing ratios occurring inside cities and with the surrounding air (Idso et al., 1998; Jacobson, 2010). The UBL also has a significant diurnal amplitude depending on temperature, moisture, and roughness, which affects air mixing: low altitudes in the early morning rise to a maximum at midday/afternoon and decrease again in the evening and night (Oke et al., 2017). According to Vogt et al. (2006), this vertical diurnal pattern of the UBL has a direct effect on the accumulation of CO_2 near the ground: when the UBL is low, compounds tend to accumulate near sources due to a lack of mixing, and when the UBL increases, pollutants scatter (Lietzke and Vogt, 2013). Furthermore, the spatial heterogeneity of land use within the UBL produces spatial variations in CO_2 (Font et al., 2015). Thus, the capacity to detect changes in CO_2 concentration from a source or sink will be local and dependent on the diurnal moment (Henninger, 2008; Strong et al., 2011).

Efforts to monitor urban CO_2 with in situ measurements include urban-wide networks of online analyzers, sensor networks and eddy covariance measurements. Several cities have implemented networks of highly sensitive instruments to measure GHGs, such as the city of Paris (Xueref-Remy et al., 2018), which started in 2010 with five measurement stations equipped with cavity ring-down spectroscopy Picarro analyzers distributed among urban, peri-urban, and rural areas. The Indianapolis Flux Experiment (INFLUX) also started in 2010 to develop and improve methods for GHG emissions from cities by employing atmospheric GHG measurements from both towers and aircraft (Davis et al., 2017). The Salt Lake Valley CO_2 Observational Network has been continuously measuring near-surface CO_2 mole fractions during the last two decades using a network of infrared gas analyzers at urban and rural sites (Pataki et al., 2003; Ehleringer et al., 2008). In cities such as Berkeley (Kim et al., 2018) and Seoul (Park et al., 2020), there are ongoing initiatives of sensor networks that measure GHG concentrations and their spatial distribution in the urban landscape, using multiple colocated sensors for calibration to improve the accuracy necessary for urban studies. With the BEASCON2N sensor network in Berkeley, McKain et al. (2012) also found that superficial measurements using commercial sensors were more sensitive to small-scale processes and increased the predictive capacity of a mesoscale model by 15 %. Eddy covariance flux (EC) measurements are used in urban areas to measure CO_2 fluxes (Velasco and Roth, 2010). The EC method is useful for determining emissions over a confined area that is directly dependent on the height of the instrument; thus, EC studies are, in most cases, limited to the neighborhood scale and cannot be extrapolated for the entire urban area. In general, observations are made in strategic locations of the urban landscape to determine the influence of geography, topography, and land-use type on CO_2 concentrations.

Several studies have attempted to understand how land use influences CO_2 mixing ratios in urban areas. For instance, Hundertmark et al. (2021) attempted to quantify the role of urban land cover in local CO_2 budgets by modeling three Boston university campuses with different landcover proportions; they found that the proportion of biogenic respiration versus anthropogenic emissions on each campus varied from 0.5 % to 2 %, representing a small fraction of overall emissions. In a study of the city of Los Angeles, Wang et al. (2022) used ground-based measurements and determined that the most important factor explaining CO_2 mixing ratios in their study was traffic reduction. A similar result was found in a recent study by Zhu et al. (2022) using ground-based observation values in the city of Shanghai, where they compared three urban land uses (green, residential and roadside) and determined that the increase in CO_2 concentrations among sites was correlated with both vegetation decrease and traffic increase.

We would like to add to this emerging field of urban in situ CO_2 observations to understand the role of land use in the urban carbon footprint by providing the results of two CO_2 measurement campaigns that occurred in the Metropolitan Area of Barcelona (AMB) during May and October 2020. Notably, during May 2020, the AMB experienced full lockdown due to COVID-19, which resulted in transport-related emission reductions of up to 75 % (Badia et al., 2021) and thus provided a better opportunity to constrain the biosphere signal than during normal activity. During October 2020, economic activity returned to normal and provided a more typical anthropogenic signal.

The overall objective of these observations is to explore how various land uses in urban regions, such as agriculture, parks, urban forests, and built areas, affect the CO_2 budget in cities while understanding the role of atmospheric processes in the transport and distribution of CO_2. As with many other cities that have signed the reduction commitment of the Paris Agreement, the AMB has committed to reducing carbon emissions by 40 % by 2030 (Barcelona's Climate Plan, 2018-2030); however, there is currently no monitoring of CO_2 to quantify the progress toward this target. The monitoring campaigns described here were strategic previous studies to determine the key measurement locations to set up the first continuous monitoring network for the AMB, and we hope its documentation will also provide useful guidance to other cities that are in the process of planning CO_2 monitoring. The CO_2 sampling campaign was funded and carried out by the ERC Consolidator project URBAG, with the overall aim of understanding the differences in carbon mixing ratios that occur throughout the day due to the heterogeneity of the urban area.

This research is the first attempt to assess the CO_2 mixing ratios and distribution of the AMB in terms of land use, orography, and atmospheric dynamics. The conclusions from this study are key in defining a future strategy for continuous CO_2 monitoring and highlight the relevance of CO_2 observations in urban planning.

2. Methods

2.1. Study site

The study area is the metropolitan area of Barcelona (hereafter referred to as the AMB), which is located in northeastern Spain (41°15'48.6"N 1°50'49.2"E: 41°32'01.7"N 2°17'46.7"E). The AMB is the second largest urban area in Spain, the 7th largest in the EU, with 636 km^2, and one of the most highly populated regions in Europe, with over 5 million inhabitants (16157 people/km^2). It is bounded by the Besos River on the North, the Llobregat River on the South, the Collserola mountain range to the West, and the Mediterranean Sea to the East, as shown in Fig. 1. Barcelona has an annual precipitation of 612 mm occurring during spring and autumn, with a mean annual temperature of 16.5 °C and a Mediterranean dry subhumid climate. The AMB is within one of the most industrialized areas in western Europe (Querol et al., 2004), where anthropogenic emissions are important contributors to GHGs, with 2.7 tons of CO_2 equivalent/capita (Harris et al., 2020). The orography of the city ranges from 0 m asl on the coastline to 512 m asl in the coastal range parallel to the sea northwest of the city. The day and night transitions of the sea/inland breeze together with the urban heat island effect cause a complex structure in the atmospheric boundary layer, modifying the temperature and dispersion of contaminants (Soler et al., 2011).

Land use in the AMB is distributed in the following manner: 58 % of the land surface (35,227 ha) is classified as green or vegetated and is composed of urban forest (47 % or 17,418 ha), peri-urban agriculture (14 %, 5500 ha) and urban parks (6 %, 2257 ha). The remaining 42 % (26,283 ha) is covered by built-up urban infrastructure (buildings, roads, industry, etc.). Land uses are shaped by physical constraints; crops are cultivated on coastal plains, and urban forests, composed of pine and Holm oaks, are located in the Collserola and El Garraf mountain ranges at relatively high altitudes (brown in the upper right map). Most of the urban area is at sea level, as shown in the map on the right (green). The urban green spaces are populated with ornamental species,

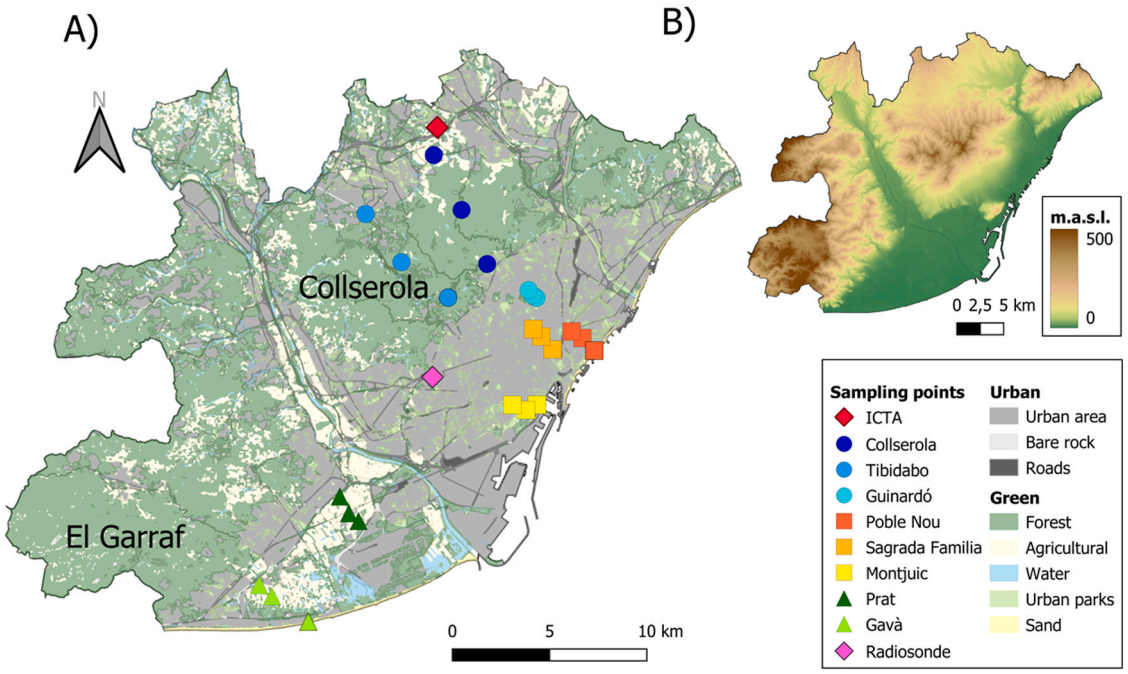

Fig. 1. Map of the metropolitan area of Barcelona showing the sampling sites. A) Land-use map with sampling locations in the AMB, based on Mendoza et al. (2023). Each sampling site is represented by a color, and the three locations of each color represent the upwind site, sampling site, and downwind site locations. B) Orographic map; different colors indicate meters above sea level (m.a.s.l.). The mountain range in the northern part of Panel A is Collserola, and the mountainous area that delimits the southwestern part in Panel A is the El Garraf mountain range.

ranging from acacias to plantain trees and ornamental shrubs and grasses, some of which are composed of invasive species. The urban green areas are scattered throughout the orography, giving rise to higher and lower areas (Fig. 1a).

2.2. Field campaign

Air samples were collected at eight sites that were strategically selected to represent the heterogeneity of land use throughout the AMB, as shown in Fig. 1a. Gavà and Prat were classified as *agricultural areas*, Tibidabo and Collserola were considered *urban forests*, Montjuic and Guinardó were considered *urban green areas*, and the last two sites, Sagrada Familia and Poble Nou, were impervious built surfaces, hereafter referred to as *urban areas* (see Table S1 for pictures and descriptions of these sites). We collected pairs of air samples at three different locations for each site, namely, the upwind site, sampling site and downwind site (hereafter referred to as upwind, site, and downwind, respectively), at the same time, simulating a Eulerian approximation in which the sampling point remained fixed (Leelőssy et al., 2016). The upwind-site-downwind trajectory was determined based on the predominant wind pattern associated with each location at that time of day and season, available from the Meteorological Service of Catalonia (https://apidocs.meteocat.gencat.cat/). The "site" location was always in the middle of the sampling trajectory (i.e., when measuring the urban green area, "site" was always inside the vegetation body), as shown in Fig. 1a. The distance between the upwind, site, and downwind locations ranged from 500 to 4000 m depending on the access for sampling and the dimensions of the item selected for study.

With the overall aim of understanding differences in CO_2 accumulation occurring between night and midday to coincide with the most intense activity of photosynthesis, we collected samples at 7:20 and 9:50 UTC for all upwind, site, and downwind locations from 18–29 in May 2020 and 15–24 in October 2020. The measurements were made on consecutive days to preserve similar atmospheric conditions as much as possible. Additional samples were collected at the Gavà, Tibidabo and Poble Nou sites at 4:20 and 11:20 UTC during the campaigns. These sites were the farthest east, north, and south, a triangle encompassing the AMB, which allowed us to determine how winds coming from different directions into the city influenced the variability in CO_2 mixing ratios. In addition to the sampling sites, online continuous CO_2 measurements were available from the ICTA building on the university campus, which is characterized by sparse buildings and greenery but has a major highway a few hundred meters away.

The first part of the campaign occurred between May 18th and June 15th, 2020, during a period of intense transport restrictions and a reduction in occupational activity in the entire AMB due to the COVID-19 pandemic. According to Google mobility reports, during these 15 days, transport mobility was 67 % less than normal at the beginning, and it slowly recovered, reaching a 49 % reduction at the end (Google, 2020). The second part of the campaign occurred from October 13th to 27th during regular economic activity and mobility. The two campaigns occurred during the growing season, which for the Mediterranean climate lasts from April until October/November. The weather was stable and sunny during both campaigns. We recorded temperature, air pressure, and wind direction and speed using a portable Skywatch (Xplorer 4) for the upwind, site and downwind locations of each site. The data are available in Table S2 in the supporting information. The relative humidity data were obtained from the Meteorological Service of Catalonia (https://apidocs.meteocat.gencat.cat/) for May and from a portable hygrometer for October (TFA Dostman GmbH & Co. KG). Air density was calculated using the air pressure, air temperature and relative humidity measured at each upwind, site, and upwind location using Eq. (1):

$$\rho = \frac{p_d}{R_d * T} + \frac{p_v}{R_v * T} \quad (1)$$

where ρ is the air density (kg/m3); p_d is the partial pressure of dry air (Pa); Rd is the specific gas constant for dry air, 287.05 J/(kg·K); T is the temperature (K); pv is the vapor pressure of water (Pa); and Rv is the specific gas constant for water vapor, 461.495 J/(kg·K). We also calculated the altitude density (AD) of each sample using an online density altitude calculator (www.omnicalculator.com) based on the

International Standard Altitude model (ISA model). AD is the height in meters above mean sea level where an air mass is located under standard atmospheric conditions according to its physical temperature, relative humidity, and pressure. In our case, we used AD to establish whether the air sample behaved as an air mass from a higher or lower altitude than where it was measured; i.e., if the sampled air had a higher AD than its measurement height, then we would expect a more well-mixed sample.

2.3. Sampling method and analysis

Two flasks per sample were collected using a sampling device that consisted of two 1-liter cylindrical borosilicate glass flasks (Normag Labor und Prozesstechnik GmbH, Germany) with Kel-F PCTFE valves fitted at both ends and a KFN air pump (Model N84.4 ANDC B - 24 V) (Fig. S1 in the supporting information). This material has shown the lowest permeation of gases compared to other sealing materials (Sturm et al., 2004). Air was collected at 3.5 m above ground level (m agl) and was pumped to the two flasks after passing through a magnesium perchlorate desiccant tube to remove moisture and a filter to remove particles. The flasks were flushed for at least 10 min, and the flow rate was recorded (between 2.0 and 3.5 L min^{-1}). After flushing, the exit valve was closed, and the flasks were pressurized with sample air to approximately 1.5 bars.

Two differential, nondispersive infrared gas analyzers (Licor7000) mounted in series were used to analyze the flask samples, and the sample measurement precision was improved by the 'in-series' configuration. Each Licor7000 analyzer measured CO_2 and H_2O vapor simultaneously on a sample and on a reference gas at a regulated flux of 0.09 L min^{-1}. The backspace between the flask valve and the analyzer inlet was emptied between measurements. Both Licor700 analyzers had been previously modified; therefore, the pressure in the sample and reference cells was adjusted by an external backpressure regulator at the end of the line to maintain constant pressure throughout the analysis time. A Valco multivalve switched between calibration standards, samples, and reference gas. The reference gas was used to calculate the drift, which was always measured between samples and/or between references. An extended explanation of the procedure and the analyzing instrumental configuration can be found in Curcoll et al. (2019). The CO_2 values that appear in this study are the mean values of both analyzers. The measurement precision improved when the two Licor7000 analyzers were used in series.

Each flask was analyzed for 7 min to avoid compromising the stability of the measurements or the flow pressure drop. Then, the calculations considered only the last 30 s. Additionally, we avoided analyzing flasks the same day they were sampled to avoid errors resulting from instrument variability and differences due to calibrations. The two Licor7000 instruments were calibrated at the beginning and at the end of the day during the analysis. We used four secondary standard cylinders that were calibrated with National Oceanic and Atmospheric Administration (NOAA) standards (WMO X2007 scale; Zhao and Tans, 2006). We estimated the uncertainties in the measured concentrations stemming from both sampling methods by using duplicate flasks in series and by using two LICOR 7000 spectrometers in series (Tans et al., 1990). The average intraflask standard deviation of both analyzers was 0.164 ppm and increased from May (0.04 ppm) to October (0.269). However, the intraflask accuracy under σ <0.2 ppm (WMO X2007 scale) was 86 % for the samples collected in October, and the total accuracy of the samples collected in May was high. The interflask variability was 0.698 ppm and was lower in May (0.237 ppm) than in October (1.044 ppm) (Table 1). Six percent of the analyses had intraf-flask σ values above 0.2 ppm, and 7 values had σ values between 1 and 2.5 ppm. These highly dispersed values corresponded to flasks with concentrations between 500 and 600 ppm, with one exception (Fig. S2). For our posterior analysis, we did not exclude any data.

In addition to the samples, we also performed online, continuous CO_2 measurements from a $CO_2/CH_4/H_2O$ PICARRO INC analyzer (G-2301) installed at the Institute de Ciència i Tecnologia Ambientals site (ICTA, 41°29'51.0"N 2°06'32.0"E, 147 m asl GHG monitoring network of the Metropolitan Area of Barcelona, www.urbag.eu/ghg/) located downwind from the Collserola range in the Vallès Occidental Valley (see Fig. 1a). An auxiliary pump was used to pump the air sampled at the rooftop to the instrument at a flow rate of 8 l/min through a 20 m 1/2" diameter Synflex piping system.

Table 1
Average (□) intra- and interflask standard deviation (σ) for all samples (Total) and for the May and October campaigns. Percentage of samples with an intra-flask precision σ <0.2 ppm (WMO X2007 scale) using the two Licor7000 analyzers in series. For a graphical representation of the CO_2 concentration (ppm) versus the standard deviation (σ), see Fig. S2.

	□ (σ Intra flask)	σ <0.2 ppm (Intra flask)	□ (σ Inter flask)
Total	**0.156±0.416**	**94 %**	**0.674±1.636**
May	0.038±0.037	100 %	0.237±0.541
October	0.290±0.578	86 %	1.045±2.236

The Picarro G-2301 instrument uses the cavity ring-down spectroscopy technique (Crosson, 2008) and measures CO_2, CH_4 and H_2O at a frequency of 1 Hz with a precision of <200 ppb for CO_2, <1.5 ppb for CH_4 and <150 ppm for H_2O according to the manufacturer's specifications (Richardson et al., 2012). Picarro values were corrected for water vapor as described by Rella et al. (2013), and a linear calibration curve was calculated every two weeks in the laboratory using four reference gases (calibration scales of WMO-CO2-X2007). The continuous measurement of CO_2 at the ICTA, which is located on the western side of the Collserola mountain range away from the city of Barcelona, allowed us to treat the ICTA site as a regional reference and compare temporal CO_2 oscillations against the samples. We averaged the values every hour on the days of the campaign and used those values as a regional reference for the CO_2 values of the AMB. The comparison between ICTA and other measurement sites can help discern between local effects and temporal effects among sites and times.

2.4. Data analysis

We represented the variability of CO_2 at the various locations and sampling times using box plots to interpret the influence of land use. K-means clustering was applied using weka software (Frank et al., 2017) to classify values from different CO_2 mixing ratios and ADs. With the clustering, we studied whether changes in CO_2 observed throughout the day were related to changes in air masses (i.e., if higher mixing ratios were grouped with similar ADs). The K-means algorithm divides the samples into K clusters of equal variances by minimizing the sum of the squared distances of the samples to their closest cluster center. The number of K clusters was chosen according to the distribution of the data as k=3, and the k groups showed well-defined differences in AD and/or mixing ratios. The cluster center is described by the mean of the samples μj (Eq. (2)):

$$\sum_{i=0}^{n} \min |x_i - \mu_j|^2 \quad (2)$$

where x_i are the data points in the cluster, μ_j is the centroid of the x_i cluster, and min $|x_i - \mu_j|^2$ assigns the data point x_i to the closest cluster judged by its sum of the squared distance from the cluster's centroid from a sample of n values.

Radiosonde measurements to calculate the planetary boundary layer (PBL) height were available at 0:00 and 12:00 UTC from the Barcelona radiosonde station (on the roof of the Faculty of Physics of the University of Barcelona at 41°23'03'' N 2°07'01''E), which is part of the Global Meteorological Network (https://public.wmo.int/en/programmes/global-observing-system). To determine the height of the PBL, we followed a robust numerical procedure proposed by Liu and Liang. (2010). A

complete explanation of the method is provided in the supplementary material (Appendix 2).

3. Results

3.1. Spatial distribution of CO2 sources and sinks

In general, there is a clear tendency for CO_2 mixing ratios to decrease as the degree of urban vegetation increases and human activity decreases. Fig. 2 reflects this trend by grouping the concentrations of the upwind, site, and downwind samples, showing the median, maximum, and minimum values for both the May and the October campaigns. During the May campaign at 7:20 UTC (9:20 local time), the CO_2 concentrations were 429 ppm and 427 ppm at the forest and agricultural sites, respectively, lower than those at the urban green sites (431 ppm for Guinardó and 471 ppm for Montjuic), and much lower than those at the urban sites (487 and 485 ppm for Poble Nou and Sagrada Familia, respectively) (see Table S2 in the supporting information for the full list of CO_2 concentrations for each site). This tendency held a few hours later at 9:50 UTC (11:50 local time, during the May campaign), when urban green sites still had higher CO_2 concentrations (431 ppm) than sites with higher agricultural and forest vegetation fractions, which had lower concentrations of 15 ppm (416 and 417 ppm, respectively).

The boxplots show more CO_2 dispersion in October than in May (on average: May 438 ±24 ppm and October 440±30 ppm). In May at 7:20 and 9:50, the mixing ratios were agricultural: 432±8 ppm and 419 ±6 ppm, urban forest: 434±14 ppm and 417±3 ppm, urban green: 452 ±22 ppm and 431±6 ppm, and urban (at 7:20 only): 482±16 ppm, respectively. In October at 7:20 and 9:50, the mixing ratios were agricultural: 439±18 ppm and 436±20 ppm, urban forest: 417±1 ppm and 415±2 ppm, urban green: 447±15 ppm and 429±10 ppm, and urban: 471±54 and 427±13 ppm, respectively. At 7:20 UTC, green and agricultural sites were 50 ppm lower than urban areas in May and 27–35 ppm lower in October. However, as morning progressed, the differences in CO_2 concentrations among the sites were not as significant in either campaign (9:50 UTC).

A decrease in CO_2 from 7:20 UTC to 9:50 UTC was observed equally at the upwind, site and downwind locations (Table S2). Higher elevations (107–442 m asl) classified as forest (Collserola 9:50, 414 ppm; Tibidabo 9:50, 419 ppm) presented lower mixing ratios. Low CO_2 concentrations were also detected in low-elevation locations (0–2 m asl) classified as agricultural sites (El Prat 9:50, 414 ppm). In general, higher altitudes and deurbanized areas had lower CO_2 mixing ratios. Three-dimensional representations of altitude, latitude (south to north) and longitude (west to east) are provided in Fig. S3 in the supporting information.

The wind roses represented in Fig. S4 in the supporting information show that, in general, for the AMB, winds in May were predominantly northwest at 4:20 UTC but were arriving from all directions at 7:20 UTC; additionally, in May, there was a change from stable to breeze conditions between 9:00 and 11:00. As the day progressed, the AMB received more wind influence from the south to southeast, with sea breezes at 9:50 and 11:20 UTC. On the other hand, during October, northwestern winds were predominant all morning until 11:20 UTC, at which point the wind speed decreased and the influence of southern winds became more prevalent. Fig. S4 shows that sea breezes started earlier in May than in October. However, local winds measured at the time of sampling were less consistent, replicating the wind pattern shown in Fig. S3, and at the microscale, we observed gusts from all directions (Fig. 3).

Additionally, Fig. 3 shows the CO_2 enhancement as the difference between the concentration at the sampling site and the ICTA location. Spatially, we observed a positive increase in CO_2 concentrations in urban areas and a negative or neutral increase in agricultural and forested areas. These differences were most significant and reached 25 ppm at 7:20 UTC (see Fig. 3a), whereas at 9:50 UTC (Fig. 3b), the increase in CO_2 was less than 10 ppm. At 7:20 UTC, locations classified as agricultural, urban forest and urban green were up to 25 ppm lower than the values recorded at the ICTA, whereas the urban impervious sampling locations (Sagrada Familia and Poble Nou) were up to 35 ppm above the ICTA reference values. It was more difficult to observe changes in CO_2 mixing ratios between locations at 9:50 UTC.

The greatest differences from the ICTA site were detected at three upwind sites in the city at 4:20 UTC. Surprisingly, both Gavà, on the coastline, and ICTA, located 14 km inland, had the highest CO_2 concentrations at 4:20, with values of 478±14 ppm and 478±20 ppm, respectively. Tibidabo recorded the lowest CO_2 values at 4:20, 425

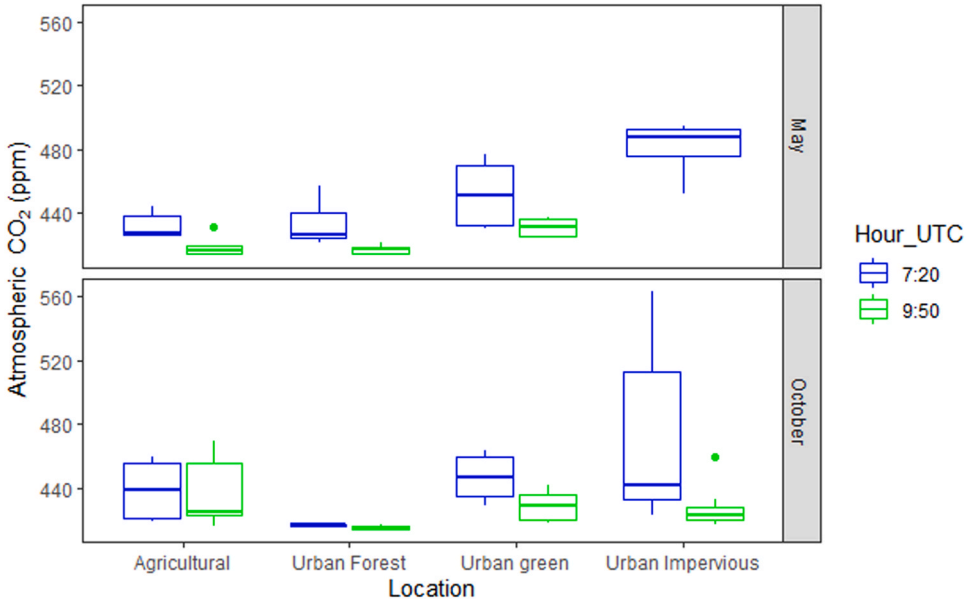

Fig. 2. Boxplots representing CO_2 concentrations at 7:20 UTC (blue) and 9:50 UTC (green) for the different land-use types in the AMB in May and October 2020. Boxplots represent the median value (horizontal line), 25th and 75th percentiles (box), and maximum and minimum values in the distribution (vertical line), and points outside the plots indicate outliers. To construct boxplots, we included all three locations (upwind, site and downwind) from both sites in each land-use category.

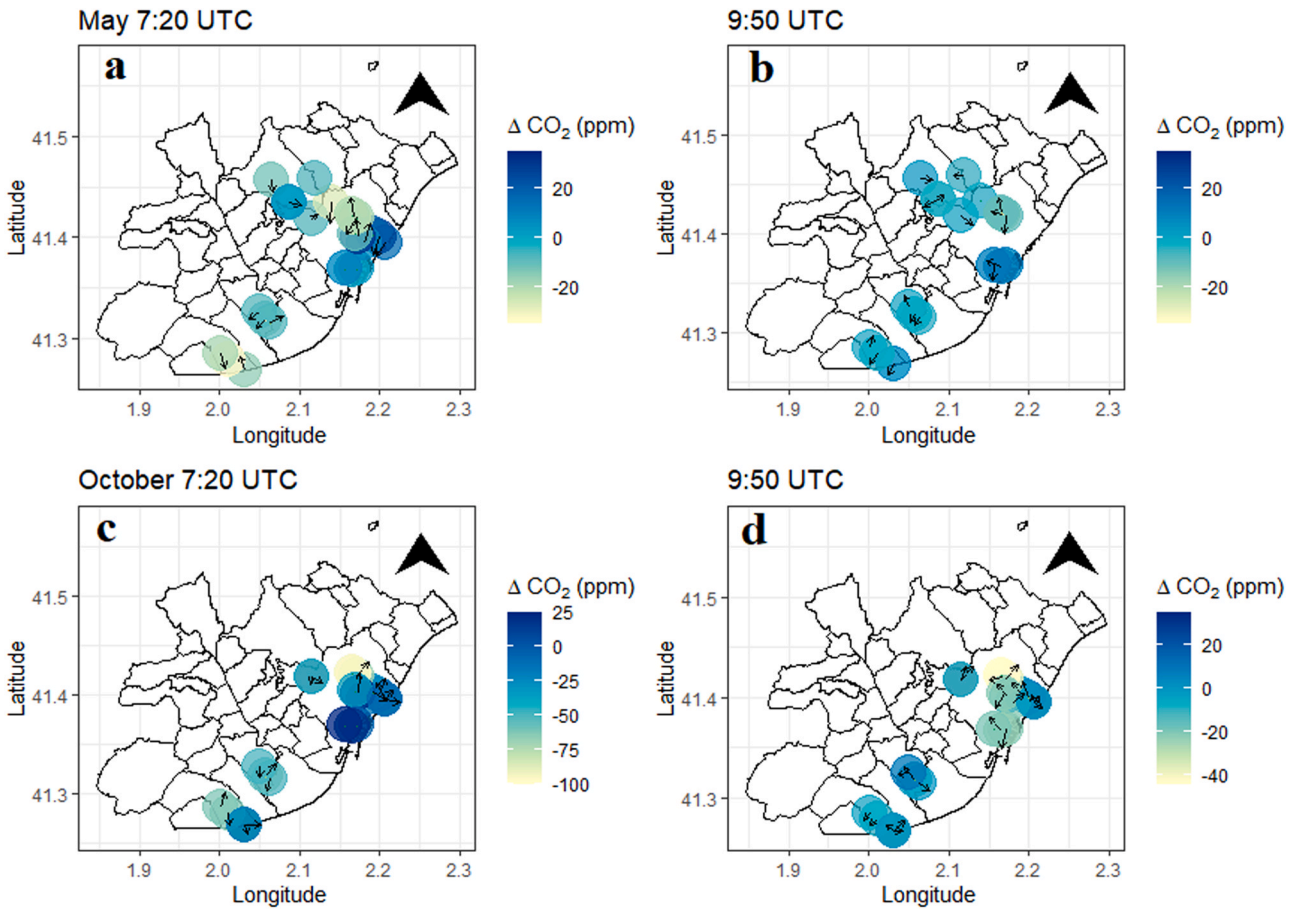

Fig. 3. Spatial representation from the sampling sites showing the increase in CO_2 at the different locations from the reference data at the ICTA site. The color gradient shows ΔCO_2, where positive values are above the reference measured at the ICTA at 7:20 (a) and 9:50 UTC (b). The arrows represent the wind directions and velocities measured in the field; the maximum speed was 2.7 m s^{-1}, and the absence of an arrow indicates that the wind velocity was 0 m/s.

±8 ppm, and Poble Nou recorded 445±23 ppm (Fig. 4). The marked differences in concentration between places were probably related to the boundary layer. Figure S5 shows that the nocturnal PBL measured at 0:00 UTC was consistently lower than 500 m for both May and October, with the exception of May 26. We believe that in our measurements at 4:20 UTC, the boundary layer remained low, leading to greater differences in the accumulation of pollutants at the different measurement sites, while as the day progressed at 7:20 and 9:50, the air dissipated. During the spring, there was greater variability and higher concentrations in the early morning at 4:20 UTC (average value of 456±28 for all sites), whereas concentrations homogenized and decreased significantly in the late morning at 11:20 UTC (average value of 418±8 for all sites). In October, the values were very similar between places, and there was less variation between night and noon than in May.

We also performed a statistical analysis of variance ANOVA to determine whether land-use type or human activity had more influence on the CO_2 concentrations. We use the measurement data of both campaigns at 7:20 UTC since this is the most complete dataset (we lack measurements of the urban impervious at 9:50 in May as can be seen in Fig. 2 of the manuscript). This time of day is also the most interesting to observe differences since it is when the PBL is still underdeveloped, and air mixing has not yet occurred- thus concentrations can be attributed to local sources and sinks. To apply the ANOVA method, we used "campaign period" and "land use" as fixed factors and the response variable is "CO_2 concentration". Mean values were compared using LSD Fisher's post-hoc test ($p<0.05$), that is a pairwise procedure to compare several treatment groups. The statistical analysis showed that there were significant differences of CO_2 concentrations between land-uses (p-value= 0.0004) independently of the campaign period. No significant differences were found for the fixed variable "campaign period" May and October (p-value=0.74) or its interaction (p-value=0.776), reflecting that land-use has more weight on the concentration variability than the campaign period. For full details of this analysis please check Supporting Information (appendix S1).

3.2. *Diurnal patterns of CO2 mixing ratios*

To understand the temporal patterns of the CO_2 mixing ratios inside the study area, we plotted discrete CO_2 concentrations sampled at the sites and the continuous concentrations at the ICTA site analyzed online by the Picarro instrument (shown in Fig. 5). In general, CO_2 from the different sampling locations (represented by dots) followed the same temporal fluctuation as that of the ICTA site, with the highest CO_2 concentrations occurring in the early morning hours and the lowest concentrations occurring at midday, as can be expected from the more developed PBL. When the values at the ICTA site were high, the values at our sampling sites were also high, with some exceptions (i.e., May 21 values of approximately 490 ppm for both the ICTA and Poble Nou and October 20 values of approximately 530 ppm for both the Sagrada Familia and the ICTA). Similarly, when we measured lower values, the ICTA also recorded lower concentrations (i.e., May 25, El prat = values of approximately 420 ppm in both places; October 20, Sagrada Familia at 9:50= values of approximately 430 in both places). The highest values of CO_2 were recorded between midnight and sunset and ranged from 440 to 480 ppm in May and up to 550 ppm in October. By midday and early afternoon, the concentrations generally decreased to

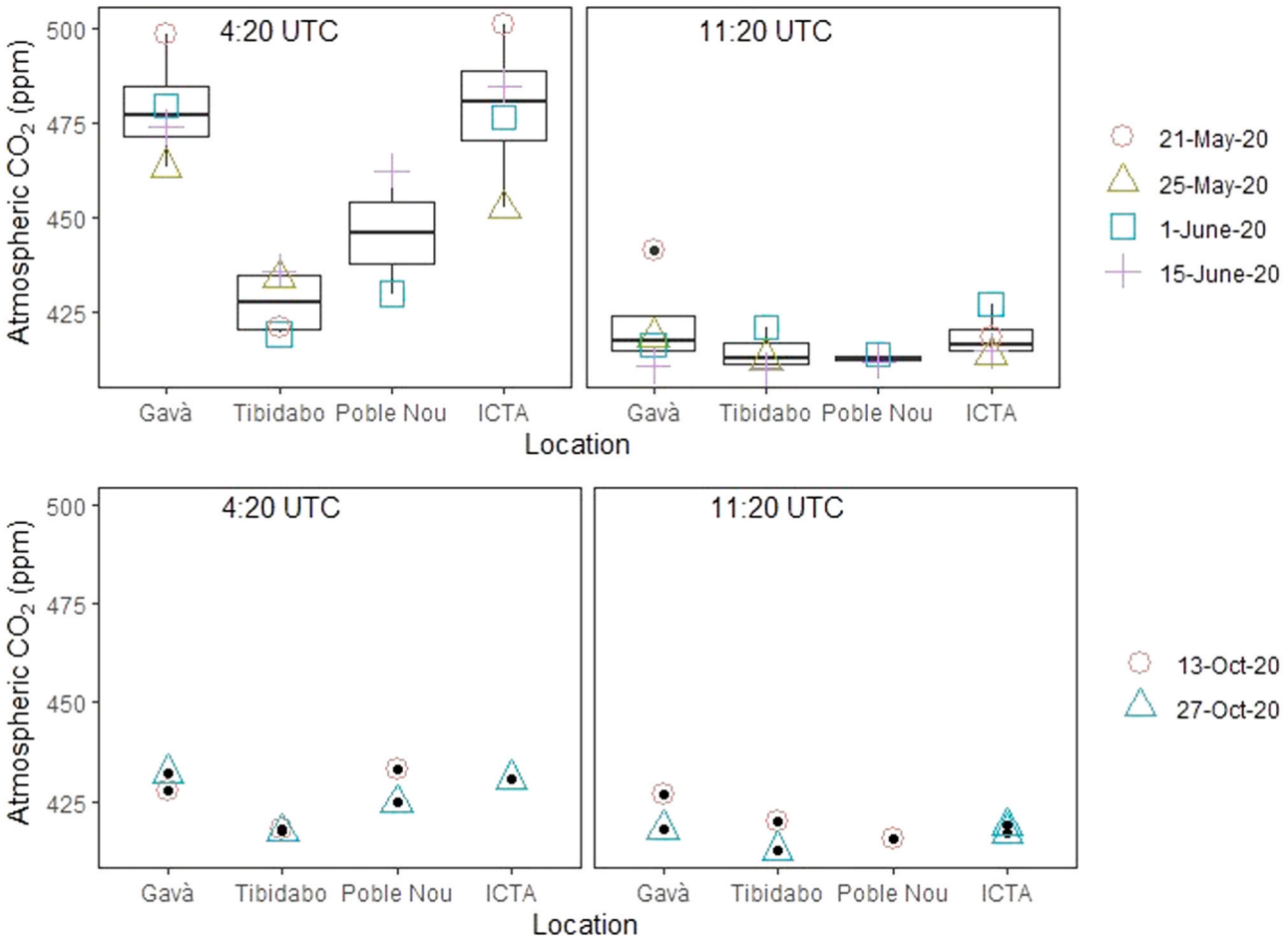

Fig. 4. Atmospheric CO_2 at the four locations surrounding the AMB at 4:20 UTC and 11:20 UTC. The figure shows the value for each day of sampling, and the boxplot represents its variation. All locations in this figure are upwind of Sampling Site A.

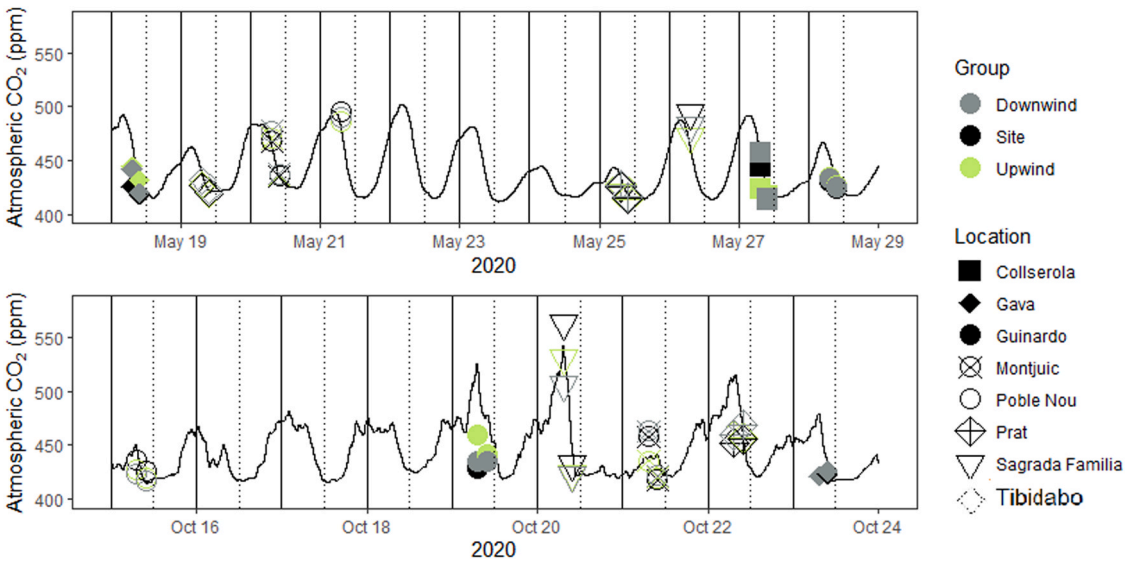

Fig. 5. Values of CO_2 mixing ratios sampled at the different locations (dots) at 7:20 and 9:50 UTC during the campaigns in May and October 2020. The solid line shows the hourly average (60 minutes running mean) CO_2 mixing ratio at the ICTA site. The solid vertical lines indicate midnight, and the dotted vertical lines indicate midday.

410–430 ppm at the ICTA. The decrease in the concentration of CO_2 between 7:20 and 9:50 was 17 ppm on average. In October, we found values that were above those of the ICTA tower at Sagrada Familia at 7:20 UTC and Montjuic and values that were below those of the ICTA tower at the Guinardó, Gavà and El Prat sampling sites, while Poble Nou recorded similar air CO_2 concentrations as the ICTA. In October, we

could say that locations with green infrastructure had lower concentrations of CO_2 at 7:20 UTC.

3.3. Changes in air masses and CO_2 mixing ratios

To understand the contribution of land use to the urban CO_2 budget, we also need to consider the influence of air transport on CO_2 concentrations throughout a city. We first evaluated the influence of the PBL on mixing ratios using values obtained from the radiosonde, as shown in Fig. S5. The PBL followed a typical day—night oscillation and ranged from approximately 300–500 m asl at night to between 700 and 1800 m asl at midday (Fig. S5). The increase in the PBL at midday matched the decrease in CO_2 observed in our measurements (Fig. 4), indicating air mixing. A comparison of Fig. S5 with Fig. 5 revealed that few days had low CO_2 concentrations (May 18 and 19 and October 23) with a developed PBL, in contrast to May 20, which had a lower PBL and higher CO_2 mixing ratios. However, on some days, such as October 20, we also obtained high CO_2 mixing ratios with high PBL development. Therefore, we can suspect that there were more factors involved in the changes in CO_2 than only in the PBL behavior.

In addition to analyzing the PBL, we also wanted to gather information about the influence of the UBL on air mass transport. Since the UBL is much more difficult to determine, we used altitude density (AD) as an indicator of the UBL since the UBL height is determined by changes in air density and heat during the day. Fig. 6 shows three regions in the air column according to the AD and CO_2 mixing ratio: 1) an upper region characterized by low CO_2 (<450 ppm) and high AD ranging between 800 and 1600 m in May and between 500 and 1500 m in October, which included all the Tibidabo sites exclusively. We hypothesized that the Tibidabo sampling sites were located in the upper layer of the UBL (the mixed layer as described by Fernando (2010)), and the low CO_2 concentrations were due to the good mixing available. 2) An intermediate region formed by low CO_2 mixing ratios (450 or lower) and low to intermediate AD, ranging from 100 to 900 m in May and from −100–500 m in October, reflecting a good mixing zone. The samples in this cluster were collected from all sites except Tibidabo, mostly at 9:50 and 11:20 UTC but also included a few samples collected at 7:20 UTC. These findings suggest that the rest of the locations were in the constant flux layer of the UBL depending on the time of day. 3) Finally, we found a third cluster or lower region, with low AD (500 m or less in both campaigns) and higher CO_2 concentrations (composed mainly of samples collected at 4:20 and 7:20 UTC from all sites but Tibidabo in May and for Montjuic, Sagrada Familia and Prat at 7:20 UTC in October). In this lower region of the UBL, such as the urban canopy layer or the roughness layer, the high CO_2 concentrations suggest CO_2 accumulation due to the reduction in air dispersion and a reduced UBL and PBL in these early morning hours. The fact that the CO_2 accumulation at 4:20 UTC was opposite between May and October could provide information on how the UBL behaves in the urban area between campaigns, although with our data, we cannot draw clear conclusions as to why this is due.

Fig. 6 also shows that the highest concentrations of CO_2 generally occurred between 4:20 and 7:20 UTC, with some discrepancies between October and May. In general, CO_2 concentrations during the morning and at sunrise showed more stratification through the AD gradient, while CO_2 concentrations decreased and AD increased throughout the morning.

4. Discussion

4.1. Sources of variability of CO_2 mixing ratios in an urban area

The main sources of CO_2 mixing ratio variability that we found during this study were land use, convection (gas transport), and the PBL. The sample measurement precision was improved by the 'in-series' configuration, and the dispersion from the analysis method was reduced to less than 0.2 ppm in 94 % of the cases, while the dispersion from the sampling collection method was 0.674±1.636 on average. This type of analysis revealed two factors. First, we achieved high precision in each individual sample analysis, which corresponds to the standards required by WMO (Crotwell and Steinbacher, 2018) for most of our samples. On the other hand, it highlights the importance of the heterogeneity that the urban environment entails and that is reflected in the collection of air samples using the double flask method, showing a variation of up to 2 ppm in the few minutes of filling each of the samples. This type of sampling is of great interest when we establish the best points to install continuous monitoring networks; therefore, it can be a very useful tool. In this study, we demonstrated the work prior to the installation of the GHG urban monitoring network for the AMB.

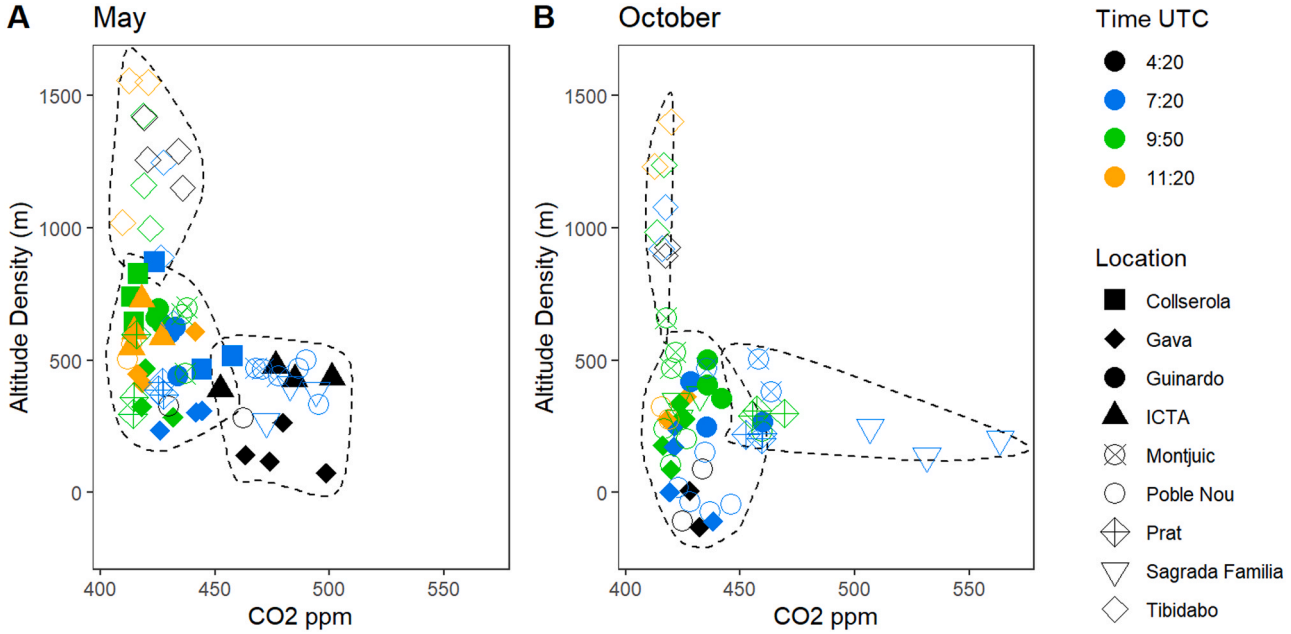

Fig. 6. Altitude density versus CO_2 mixing ratios at the field sites in May and October. Dotted areas represent the 3 clusters or groups obtained for each period using the k-means algorithm.

4.2. Land use

In terms of land use, we generally found higher CO_2 concentrations inside urban areas (e.g., Sagrada Familia, Poble Nou, and Montjuic) than in suburban or peri-urban areas (Gavà, Collserolla, and Tibidabo). In terms of land use, urban sites (Poble Nou and Sagrada Familia) contributed 31 ppm more CO_2 than did ICTA, while agricultural sites contributed up to 50 ppm less CO_2, forest sites contributed 26 ppm less CO_2 and urban green sites contributed up to 60 ppm less CO_2 than did ICTA (Fig. 3). This trend of lower values of CO_2 in forested and agricultural areas and higher values in urban areas is consistent with other urban studies that have found higher CO_2 emissions in downtown, impervious urban areas (i.e., CO_2 emission distribution in the Toronto area, Pugliese et al., 2018) and lower values in forested spaces (Briber et al., 2013). Bergeron and Strachan found a clear decrease in CO_2 fluxes from urban to suburban and agricultural areas in Montreal and concluded that the lower emissions were due to vehicular traffic contributions decreasing from 11.5 μmol m^{-2} s^{-1} in urban areas to 4.8 μmol m^{-2} s^{-1} in suburban areas (Bergeron and Strachan, 2011). Lee et al. (2017) found, using eddy covariance, that downtown areas emitted 3–5 times more CO_2 than did peripheral areas and that mixing ratios increased by 24–39 ppm from green suburban areas to downtown areas. Our study revealed an average decrease of 35 ppm in the CO_2 mixing ratio as we approached suburban areas compared to downtown areas, which was linked to this vehicular reduction occurring from urban to suburban areas.

Consistent with our results, Da Silva et al. (2019) suggested that urban forests contribute to CO_2 mitigation by a dilution effect from the urban emissions that are produced in less populated areas, and an efficient spatial mixing of air masses that decreases mixing ratios by 4–5 %; in our case, a reduction from urban to peri-urban (forest and agricultural) areas, was on the order of 4–7 %. A trend toward CO_2 reduction in the suburban areas was observed during the day but not at night at sites such as Gavà and ICTA, which experienced high CO_2 accumulation at 4:20 UTC in May and were much greater than those at the urban site in Poble Nou during the same hour. This increase in CO_2 during the night could be the result of an accumulation of CO_2 from plant respiration in Gavà and/or industrial activity in the Vallès area near the ICTA site, which accumulated pollutants despite the decrease in the UBL at night. Poble Nou received less local emissions from biogenic (trees) or anthropogenic (traffic) sources at 4:20 due to low green areas and the reduction in transport at night.

Another factor affecting the CO_2 mixing ratio was the altitude. We observed CO_2 concentrations up to 40 ppm lower in the Tibidabo upwind location (the highest location at 442 m asl) than in other locations sampled at the same time but at sea level, such as Gavà and Poble Nou (~0 m asl). The Tibidabo location, which always had lower concentrations, was more affected by upper cleaner air masses than the other locations. We can explain this decrease in mixing ratios by a combination of factors such as the contribution of the urban biosphere to CO_2 capture (forest) and a reduction in anthropogenic activities such as traffic in this area, as well as by the increase in air mixing resulting from a higher altitude compared to the rest of the locations. That is, Tibidabo could be located above the UBL. Gao et al. (2018) found a similar gradient in a transect in the city of Najin, China (0–110 m agl), and attributed the difference in CO_2 to the presence of two air masses with different mixing ratios. These authors attributed the decrease in CO_2 between 65 and 110 m a.g.l. to efficient mixing ratio phenomena occurring under the UBL, which could be the same for us at the Tibidabo location.

4.3. Sources and sinks: fuel combustion and urban vegetation

In terms of local processes, we investigated how CO_2 mixing ratios are influenced by CO_2 uptake and emissions from urban vegetation and fuel combustion processes, both domestic and industrial, including marine ports. The sources and sinks of CO_2 mixing ratios in the AMB can be attributed to local processes because the wind speed never exceeded 2.7 m s^{-1} during the two campaigns. A similar behavior was noted in a recent study by Xueref-Remy et al. (2018) for the city of Paris, where local CO_2 sources were clearly detected when wind speeds were lower than 3 m s^{-1}, while winds between 3 and 9 m s^{-1} were able to capture the effect of city emissions at urban stations but not at rural sites.

Although the net capacity for CO_2 uptake by the urban biosphere is still not well known, our study is consistent with others in that the contribution of urban green areas to reducing CO_2 concentrations is significant. Bergeron and Strachan (2011) found a change from source to a slight sink of CO_2 by increasing vegetation presence when moving from urban (emitting 204 t CO_2 ha^1 $year^1$), suburban (emitting 54 t CO_2 ha^1 $year^1$) to agricultural areas (capturing 2 t CO_2 ha^1 $year^1$) in Montreal. Similarly, for the city of Boston, Briber et al. (2013) observed that increasing vegetation reduced the CO_2 mixing ratio by an average of 6.7 ppm compared to that in the urban sector when surrounded by forest, but there were no differences in heterogeneous suburban areas. In our case, the CO_2 mixing ratios also decreased when moving away from urban to peri-urban areas, but this phenomenon could also be related to anthropogenic activity reduction occurring as we moved from highly traffic-congested areas; however, during the lockdown, this was not the case in May. In our case, the urban sites had the highest CO_2 ratios, at 458± 41 ppm on average, and we also found that the urban parks had lower CO_2 ratios (439± 17 ppm) than did their neighboring all-urban areas. This can be interpreted in two ways: 1. the urban biosphere contributing to the absorption of CO_2 and 2. an increase in the distance of the emission focus. This indicates that the urban biosphere contributes to the uptake of CO_2 directly through C uptake but also indirectly through the creation of spaces with lower anthropogenic activity. Finally, agricultural sites (432± 16 ppm) and forests (423± 12 ppm) had the lowest concentrations.

However, differences were clearer in May than in October and mostly occurred at 7:20 UTC, as represented in Fig. 2, which could be attributed to the reduction in anthropogenic activity occurring during that period. We found more dispersion in October than in May; one explanation is most likely the 40–60 % reduction in mobility during May (Badia et al., 2021), which permitted better capture of the biogenic signal. Additionally, there was a very clear decrease in CO_2 concentrations as the day progressed from 7:20–9:50 UTC, which we mostly attributed to the development of the PBL favoring air mixing.

In fact, Kennedy et al. (2009) estimated that ground transportation in the city of Barcelona accounted for 28 % of total GHG emissions, which is expected to decrease by 15 % from the current emissions related to changes in mobility, with an increase in electric vehicles (BCN, 2022). With the reduction in transportation in May 2020, the estimated contribution of total GHG emissions was still 12–17 % of that in October 2020. Other sources of emissions in the city of Barcelona were determined to be essential industrial activities (i.e., transport and production of first-need supplies) that did not decrease during May. On the other hand, aviation was described as the major source in Kennedy et al. (2009), and it decreased during the pandemic. However, the difference in activity did not translate to a general increase in the average CO_2 mixing ratio between May (439±26 ppm) and October. That is, when we examined in detail mixing ratios at urban sites, we observed a decrease from May to October, but at the same time, dispersion increased (from 481± 16 ppm to 471± 54 ppm, comparison at 7:20 UTC since we lacked data at 9:50 in May), while there was no clear explanation for a decrease in concentration (i.e., it could be due to differences in the PBL, changes in biogenic and anthropogenic contributions, and changes in the CO_2 background); the increase in dispersion may be related to a greater quantity of sources since anthropogenic activities returned to normal. The increase in both concentration and dispersion was similar for urban green sites (from 425±9 ppm in May to 437±19 ppm in October). At the forest sites, we observed that the CO_2 concentration decreased from 425 ±12 ppm to 416±2 ppm, and at the agricultural sites, the CO_2

concentration decreased from 441±18 ppm to 437±15 ppm from May to October. In both cases, dispersion was maintained at a similar level or decreased. It seems that the increase in dispersion in urban areas (urban and urban green areas) was due to heterogeneous sources of CO_2 that were present in October but suppressed in May with the lockdown restrictions.

4.4. Convection, PBL, UBL and local winds

Our study also helped us understand the atmospheric dynamics occurring in the AMB and their repercussions on the CO_2 distribution. The diurnal concentration differences can be explained by the increase in air mixing that occurs during the day due to the development of the PBL. The accumulation of CO_2 generally occurs at night and in the early morning when a low PBL prevents air mixing. We clearly observed a diurnal decrease in CO_2 of 95 ±27 ppm from 4:20 UTC to 11:20 UTC (Fig. 4). The air column formed at night-time remains stable early in the morning, maintains local air accumulation associated with atmospheric stratification (Briber et al., 2013), and disappears late at noon as convective processes develop and produce air mixing. This process of air accumulation is enhanced in cities by surface discontinuities created by street canyons, together with the direct effect of UBL height on accumulation and dilution (Lietzke and Vogt, 2013). We estimate that the best moment to determine sources of CO_2 is during the early morning, characterized by a low boundary layer height and air accumulation near the ground.

In our study, we used air altitude density as an indicator of the UBL (Fig. 6), rationalizing that high altitude densities indicate a high zone in the UBL (such as the mixed layer or the constant flux layer, as designated by Fernando (2010)), where air masses may have mixed with upper air, whereas low altitude densities suggest local air masses, low mixing, and therefore a lower UBL zone such as the rough sublayer. We found differences in air density and established three clearly distinct clusters characterized by differences in CO_2 concentrations, which indicate three different zones of the UBL. We observed that air mass samples from urbanized areas with low AD values had elevated CO_2 concentrations, suggesting an accumulation of CO_2 and a reduction in vertical air mixing, as is found within the urban canopy layer of the UBL. These findings agree with a study by Font et al. (2015), who determined that London buildings reduced air mixing, and another study by Jacobson (2010), who reported that the CO_2 mixing ratios of air masses affected by the city were 75 % greater than those in the surrounding areas due to processes that favor the accumulation of air with high levels of CO_2, known as urban domes, which consist of higher mixing ratios formed over the influence of an urban area.

According to Song and Wang (2016), green infrastructure can modify the UBL height due to their thermoregulation capacity. Regarding green areas, we found examples of strong diurnal variability; for instance, at Montjuic and Collserola, CO_2 values decreased by 30 ppm from 7:20–9:50 UTC. At the same time, the AD also increased at approximately 200–300 m, indicating the entrance of different air masses with relatively high mixing rates. Vogt et al. (2006) reported similarities in the diurnal variability of mixing ratios in the city of Basel, Switzerland; they found that the maximum values of CO_2 between 5:00 and 7:00 UTC progressively decreased until noon. The maximum values between 4:20 and 7:20 UTC decreased between 9:50 and 11:20 UTC.

The accumulation of CO_2 at coastal locations is further explained by the formation of an urban dome over the AMB and the sea, causing urban air accumulation during the night on the coastline, which is recirculated back to the city with sea breezes that pick up mid-morning (see Grossi et al. (2000) for a full description of this phenomenon). Urban domes are formed by the UBL in the absence of regional winds, and when they occur, the climatic influence of a city is restricted to a self-contained urban dome (Martilli, 2003; Oke et al., 2017). This was clearly seen at 4:20 UTC in May at Gavà, where concentrations were between 470 and 500 ppm. Finally, when measuring atmospheric CO_2, another important factor to consider is how the local wind and breezes affect the air sample at the moment of measurement. In our case, one example of local accumulation at 4:20 UTC (Fig. 5) in Gavà was accompanied by the occurrence of inland winds, as shown by the wind roses in Fig. S4 in the supplementary information, when greater increases in CO_2 in the urban area occurred during a time of calm winds in Montjuic that could have enhanced the accumulation of pollutants from the surroundings (i.e., main roads nearby and port activity).

5. Conclusions

In this study, we attempted to contribute to one of the main challenges in urban CO_2 monitoring: how to properly attribute the variability of CO_2 mixing ratios to the various factors that influence them: the urban landscape, local processes, geography, and atmospheric dynamics, among others. Our analysis of the CO_2 sampling campaigns over the Metropolitan Area of Barcelona (AMB) revealed that CO_2 mixing decreased as a combination of the degree of anthropogenic activity decreased and urban vegetation increased when comparing land uses. We found that intensely urbanized areas had the highest CO_2 concentrations (458±41 ppm) and that green areas had significantly lower CO_2 concentrations proportional to the vegetation volume: urban forest (423 ±12 ppm), peri-urban agriculture (439±16 ppm), and urban parks (439 ±17). Overall, land use and local processes had important influences on CO_2 mixing ratios. We examined spatial and diurnal changes in atmospheric CO_2 concentrations compared to the reference CO_2 concentrations outside the urban area (at the UAB campus and ICTA building), which allowed intercomparisons among days. As a general rule, sampling sites located in areas with more vegetation and less traffic or industrial activity had lower CO_2 concentrations, and impervious urbanized areas had CO_2 concentrations above the background values.

The sampling campaign also provided some insight into the atmospheric dynamics inside the city, such as the importance of the wind (mesoscale and local), PBL and UBL. Low boundary layers were related to the increase in CO_2 accumulation near the surface, mostly during the night-time or early morning, creating three clusters characterized by different altitude densities (ADs). We suggest the use of the UBL as an indicator to characterize different air masses and CO_2 mixing ratios. Examples of local CO_2 accumulation were accompanied by the occurrence of inland winds, although the link between local winds and emission sources was not determined.

Based on these campaigns, we recommend continuous monitoring of CO_2 concentrations to better capture diurnal and seasonal patterns and that the monitoring be well distributed to capture the various land uses and various zones of the UBL. As seen in this study, land use may determine the accumulation and dispersion of pollutants inside urban areas since it affects both emission factors (i.e., vegetation and traffic) and atmospheric behavior (the UBL and local winds). We also believe that it is important to increase the spatiotemporal resolution and extend surface observations to better characterize the urban environment.

CRediT authorship contribution statement

Roger Curcoll: Writing – review & editing, Methodology, Data curation. **Carme Estruch:** Writing – review & editing, Writing – original draft, Methodology, Formal analysis, Data curation. **Gara Villalba:** Writing – review & editing, Writing – original draft, Investigation, Funding acquisition, Formal analysis, Data curation, Conceptualization. **Joan Gilabert:** Methodology, Data curation. **Alba Badia:** Methodology, Data curation. **Ricard Segura-Barrero:** Methodology, Data curation. **Josep Anton Morgui:** Methodology, Data curation, Conceptualization. **Veronica Vidal:** Methodology, Data curation. **Sergi Ventura:** Methodology, Data curation.

Declaration of Competing Interest

The authors declare the following financial interests/personal relationships which may be considered as potential competing interests: Gara Villalba reports financial support was provided by Autonomous University of Barcelona. If there are other authors, they declare that they have no known competing financial interests or personal relationships that could have appeared to influence the work reported in this paper.

Acknowledgements

This study has been carried out thanks to the financial support of the ERC Consolidator grant: Integrated System Analysis of Urban Vegetation and Agriculture (818002-URBAG), of the European Commission, Horizon 2020 Program. The authors would also like to thank the support of the Spanish Ministry of Science, Innovation and Universities, through the "Maria de Maeztu" programme for Units of Excellence (CEX2019–000940-M).

Appendix A. Supporting information

Supplementary data associated with this article can be found in the online version at doi:10.1016/j.ufug.2024.128438.

References

Badia, A., Langemeyer, J., Codina, X., Gilabert, J., Guilera, N., Vidal, V., Segura, R., Vives, M., Villalba, G., 2021. A take-home message from COVID-19 on urban air pollution reduction through mobility limitations and teleworking. npj Urban Sustain. 1 https://doi.org/10.1038/s42949-021-00037-7.

BCN: Pla d'acció d'emergencia climàtica 2030, 2022.

Bergeron, O., Strachan, I.B., 2011. CO2 sources and sinks in urban and suburban areas of a northern mid-latitude city. Atmos. Environ. 45, 1564–1573. https://doi.org/10.1016/j.atmosenv.2010.12.043.

Briber, B.M., Hutyra, L.R., Dunn, A.L., Raciti, S.M., Munger, J.W., 2013. Variations in atmospheric CO2 mixing ratios across a Boston, MA urban to rural gradient. Land (Basel) 2, 304–327. https://doi.org/10.3390/land2030304.

Barcelona's Climate Plan 2018 - 2030: https://www.barcelona.cat/barcelona-pel-clima/en.

Covenant of Mayors: Covenant of Mayors Official Text, 2009.

Crosson, E.R., 2008. A cavity ring-down analyzer for measuring atmospheric levels of methane, carbon dioxide, and water vapor. Appl. Phys. B 92, 403–408. https://doi.org/10.1007/s00340-008-3135-y.

Crotwell, A., Steinbacher, M., 2018. 19th WMO/IAEA Meeting on Carbon Dioxide, Other Greenhouse Gases and Related Tracers Measurement Techniques (GGMT-2017). GAW Report. https://doi.org/10.1016/j.yhbeh.2013.09.005.

Curcoll, R., Camarero, L., Bacardit, M., Àgueda, A., Grossi, C., Gacia, E., Font, A., Morguí, J.-A., 2019. Atmospheric Carbon Dioxide variability at Aigüestortes, Central Pyrenees, Spain. Reg. Environ. Change 19, 313–324. https://doi.org/10.1007/s10113-018-1443-2.

Davis, K.J., Deng, A., Lauvaux, T., Miles, N.L., Richardson, S.J., Sarmiento, D.P., Gurney, K.R., Hardesty, R.M., Bonin, T.A., Brewer, W.A., Lamb, B.K., Shepson, P.B., Harvey, R.M., Cambaliza, M.O., Sweeney, C., Turnbull, J.C., Whetstone, J., Karion, A., 2017. The Indianapolis Flux Experiment (INFLUX): A test-bed for developing urban greenhouse gas emission measurements. Elementa 5. https://doi.org/10.1525/elementa.188.

Ehleringer, J., Schauer, A.J., Lai, C.-T., Bowling, D.R., Pataki, D.E., Stephens, B.B., 2008. Long-term carbon dioxide monitoring in Salt Lake City. Eos Trans. AGU, Fall Meet. Suppl., Abstr. B43D–B40466.

European Commission: The European Green Deal, 2019.

Fernando, H.J.S., 2010. Fluid Dyn. Urban atmospheres Complex Terrain. https://doi.org/10.1146/annurev-fluid-121108-145459.

Font, A., Grimmond, C.S.B., Kotthaus, S., Morguí, J.A., Stockdale, C., O'Connor, E., Priestman, M., Barratt, B., 2015. Daytime CO2 urban surface fluxes from airborne measurements, eddy-covariance observations and emissions inventory in Greater London. Environ. Pollut. 196, 98–106. https://doi.org/10.1016/j.envpol.2014.10.001.

Frank, E., Hall, M.A., Witten, I.H., 2017. The WEKA workbench. Data Min. 553–571. https://doi.org/10.1016/b978-0-12-804291-5.00024-6.

Gao, Y., Lee, X., Liu, S., Hu, N., Wei, X., Hu, C., Liu, C., Zhang, Z., Yang, Y., 2018. Spatiotemporal variability of the near-surface CO2 concentration across an industrial-urban-rural transect, Nanjing, China. Sci. Total Environ. 631–632, 1192–1200. https://doi.org/10.1016/j.scitotenv.2018.03.126.

Google: Google COVID-19 Community Mobility Report, 2020.

Grossi, P., Thunis, P., Martilli, A., Clappier, A., 2000. Effect of Sea Breeze on Air Pollution in the Greater Athens Area. Part II: Analysis of Different Emission Scenarios. J. Appl. Meteorol. 39, 563–575. https://doi.org/10.1175/1520-0450(2000)039<0563:EOSBOA>2.0.CO;2.

Harris, S., Weinzettel, J., Bigano, A., Källmén, A., 2020. Low carbon cities in 2050? GHG emissions of European cities using production-based and consumption-based emission accounting methods. J. Clean. Prod. 248 https://doi.org/10.1016/j.jclepro.2019.119206.

Henninger, S., 2008. Analysis of near surface CO<inf>2</inf> variability within the urban area of Essen, Germany. Meteorol. Z. 17, 19–27. https://doi.org/10.1127/0941-2948/2008/0261.

Hundertmark, W.J., Lee, M., Smith, I.A., Bang, A.H.Y., Chen, V., Gately, C.K., Templer, P. H., Hutyra, L.R., 2021. Influence of landscape management practices on urban greenhouse gas budgets. Carbon Balance Manag. 16, 1–12. https://doi.org/10.1186/s13021-020-00160-5.

Idso, C.D., Idso, S.B., Balling, R.C., 1998. The urban CO2 dome of phoenix. Ariz., Phys. Geogr. 19, 95–108. https://doi.org/10.1080/02723646.1998.10642642.

IEA, 2016. Cities are in the Frontline for Cutting Carbon Emissions. International Energy Agency.

Jacobson, M.Z., 2010. Enhancement of local air pollution by urban CO2 domes. Environ. Sci. Technol. 44, 2497–2502. https://doi.org/10.1021/es903018m.

Kennedy, C., Steinberger, J., Gasson, B., Hansen, Y., Hillman, T., Havránek, M., Pataki, D., Phdungsilp, A., Ramaswami, A., Mendez, G.V., 2009. Greenhouse gas emissions from global cities. Environ. Sci. Technol. 43, 7297–7302. https://doi.org/10.1021/es900213p.

Kim, J., Shusterman, A.A., Lieschke, K.J., Newman, C., Cohen, R.C., 2018. The Berkeley Atmospheric CO2 Observation Network: Field calibration and evaluation of low-cost air quality sensors. Atmos. Meas. Tech. 11, 1937–1946. https://doi.org/10.5194/amt-11-1937-2018.

Lee, J.K., Christen, A., Ketler, R., Nesic, Z., 2017. A mobile sensor network to map carbon dioxide emissions in urban environments. Atmos. Meas. Tech. 10, 645–665. https://doi.org/10.5194/amt-10-645-2017.

Leelőssy, Á., Mona, T., Mészáros, R., Lagzi, I., Havasi, Á., 2016. Eulerian Lagrangian Approaches Model. Air Qual. https://doi.org/10.1007/978-3-319-40157-7_5.

Lietzke, B., Vogt, R., 2013. Variability of CO2 concentrations and fluxes in and above an urban street canyon. Atmos. Environ. 74, 60–72. https://doi.org/10.1016/j.atmosenv.2013.03.030.

Liu, S., Liang, X.-Z., 2010. Observed Diurnal Cycle Climatology of Planetary Boundary Layer Height. J. Clim. 23, 5790–5809. https://doi.org/10.1175/2010JCLI3552.1.

Martilli, A., 2003. A Two-Dimensional Numerical Study of the Impact of a City on Atmospheric Circulation and Pollutant Dispersion in a Coastal Environment. Bound. -Layer. Meteorol. 108, 91–119. https://doi.org/10.1023/A:1023044100064.

McHale, M.R., Gregory McPherson, E., Burke, I.C., 2007. The potential of urban tree plantings to be cost effective in carbon credit markets. Urban For. Urban Green. 6, 49–60. https://doi.org/10.1016/j.ufug.2007.01.001.

McKain, K., Wofsy, S.C., Nehrkorn, T., Eluszkiewicz, J., Ehleringer, J.R., Stephens, B.B., 2012. Assessment of ground-based atmospheric observations for verification of greenhouse gas emissions from an urban region. Proc. Natl. Acad. Sci. 109, 8423–8428. https://doi.org/10.1073/pnas.1116645109.

Mendoza, A., Padró, R., La Rota-Aguilera, M.J., Marull, J., Eckelman, M.J., Cirera, J., Giocoli, A., Villalba, G., 2023. Displaying geographic variability of peri-urban agriculture environmental impacts in the Metropolitan Area of Barcelona: A regionalized life cycle assessment. Sci. Total Environ. 858, 159519 https://doi.org/10.1016/j.scitotenv.2022.159519.

Oke, T.R., 1976. The distinction between canopy and boundary-layer urban heat Islands. Atmosphere (Basel) 14, 268–277. https://doi.org/10.1080/00046973.1976.9648422.

Oke, T.R., Columbia, B., Climates, B.L., Climate, U., Service, M., Medal, P., Canadian, R., Society, G., Medal, M., Mills, G., Society, G., Climate, U., Christen, A., Program, A.S., Columbia, B., Voogt, J.A., Prediction, E., and Network, C.C.: Urban Climates by T.R. Oke, G. Mills, A. Christen, J.A. Voogt (z-lib.org).pdf, 2017.

Park, C., Jeong, S., Park, H., Woo, J.-H., Sim, S., Kim, J., Son, J., Park, H., Shin, Y., Shin, J.-H., Kwon, S.-M., Lee, W.-Y., 2020. Challenges in Monitoring Atmospheric CO2 Concentrations in Seoul Using Low-Cost Sensors. Asia-Pac. J. Atmos. Sci. https://doi.org/10.1007/s13143-020-00213-2.

Pataki, D.E., Bowling, D.R., Ehleringer, J.R., 2003. Seasonal cycle of carbon dioxide and its isotopic composition in an urban atmosphere: Anthropogenic and biogenic effects. J. Geophys. Res.: Atmospheres 108. https://doi.org/10.1029/2003jd003865.

Pugliese, S.C., Murphy, J.G., Vogel, F.R., Moran, M.D., Zhang, J., Zheng, Q., Stroud, C.A., Ren, S., Worthy, D., Broquet, G., 2018. High-resolution quantification of atmospheric CO2 mixing ratios in the Greater Toronto Area. Can., Atmos. Chem. Phys. 18 https://doi.org/10.5194/acp-18-3387-2018.

Querol, X., Alastuey, A., Ruiz, C.R., Artiñano, B., Hansson, H.C., Harrison, R.M., Buringh, E., Ten Brink, H.M., Lutz, M., Bruckmann, P., Straehl, P., Schneider, J., 2004. Speciation and origin of PM10 and PM2.5 in selected European cities. Atmos. Environ. 38, 6547–6555. https://doi.org/10.1016/j.atmosenv.2004.08.037.

Rahman, M.A., Stratopoulos, L.M.F., Moser-Reischl, A., Zölch, T., Häberle, K.H., Rötzer, T., Pretzsch, H., Pauleit, S., 2020. Traits of trees for cooling urban heat islands: A meta-analysis. Build. Environ. 170 https://doi.org/10.1016/j.buildenv.2019.106606.

Rella, C.W., Chen, H., Andrews, A.E., Filges, A., Gerbig, C., Hatakka, J., Karion, A., Miles, N.L., Richardson, S.J., Steinbacher, M., Sweeney, C., Wastine, B., Zellweger, C., 2013. High accuracy measurements of dry mole fractions of carbon dioxide and methane in humid air. Atmos. Meas. Tech. 6, 837–860. https://doi.org/10.5194/amt-6-837-2013.

Richardson, S.J., Miles, N.L., Davis, K.J., Crosson, E.R., Rella, C.W., Andrews, A.E., 2012. Field testing of cavity ring-down spectroscopy analyzers measuring carbon dioxide and water vapor. J. Atmos. Ocean. Technol. 29 https://doi.org/10.1175/JTECH-D-11-00063.1.

da Silva, C.M., da Silva, L.L., Souza, T., de, C., Dantas, T.C., Corrêa, S.M., Arbilla, G., 2019. Main Greenhouse Gases levels in the largest secondary urban forest in the world. Atmos. Pollut. Res. 10, 564–570. https://doi.org/10.1016/j.apr.2018.10.009.

Soler, M.R., Arasa, R., Merino, M., Olid, M., Ortega, S., 2011. Modelling Local Sea-Breeze Flow and Associated Dispersion Patterns Over a Coastal Area in North-East Spain: A Case Study. Bound. -Layer. Meteorol. 140 https://doi.org/10.1007/s10546-011-9599-z.

Song, J., Wang, Z.-H., 2016. Diurnal changes in urban boundary layer environment induced by urban greening. Environ. Res. Lett. 11 https://doi.org/10.1088/1748-9326/11/11/114018.

Strong, C., Stwertka, C., Bowling, D.R., Stephens, B.B., Ehleringer, J.R., 2011. Urban carbon dioxide cycles within the Salt Lake Valley: A multiple-box model validated by observations. J. Geophys. Res. Atmospheres 116. https://doi.org/10.1029/2011JD015693.

Sturm, P., Leuenberger, M., Sirignano, C., Neubert, R.E.M., Meijer, H.A.J., Langenfelds, R., Brand, W.A., Tohjima, Y., 2004. Permeation of atmospheric gases through polymer O-rings used in flasks for air sampling. J. Geophys. Res. D: Atmospheres 109.

Tans, P.P., Fung, I., Takahashi, T., 1990. Observational Constraints on the Global Atmospheric CO2 Budget. Science 247 (1979), 1431–1439. https://doi.org/10.1126/science.247.4949.1431.

Velasco, E., Roth, M., 2010. Cities Net. Sources CO2: Rev. Atmos. CO2 Exch. Urban Environ. Meas. eddy covariance Tech. https://doi.org/10.1111/j.1749-8198.2010.00384.x.

Villalba, G., Whelan, M., Montzka, S.A., Cameron-Smith, P.J., Fischer, M., Zumkehr, A., Hilton, T., Stinecipher, J., Baker, I., Bambha, R.P., Michelsen, H.A., LaFranchi, B.W., Estruch, C., Campbell, E., 2021. Exploring the Potential of Using Carbonyl Sulfide to Track the Urban Biosphere Signal. J. Geophys. Res.: Atmospheres 126. https://doi.org/10.1029/2020JD034106.

Vogt, R., Christen, A., Rotach, M.W., Roth, M., Satyanarayana, A.N.V., 2006. Temporal dynamics of CO2 fluxes and profiles over a Central European city. Theor. Appl. Climatol. 84, 117–126. https://doi.org/10.1007/s00704-005-0149-9.

Wang, H., Gong, F.Y., Newman, S., Zeng, Z.C., 2022. Consistent weekly cycles of atmospheric NO2, CO, and CO2 in a North American megacity from ground-based, mountaintop, and satellite measurements. Atmos. Environ. 268 https://doi.org/10.1016/j.atmosenv.2021.118809.

Xu, C., Dong, L., Yu, C., Zhang, Y., Cheng, B., 2020. Can forest city construction affect urban air quality? The evidence from the Beijing-Tianjin-Hebei urban agglomeration of China. J. Clean. Prod. 264, 121607 https://doi.org/10.1016/j.jclepro.2020.121607.

Xueref-Remy, I., Dieudonné, E., Vuillemin, C., Lopez, M., Lac, C., Schmidt, M., Delmotte, M., Chevallier, F., Ravetta, F., Perrussel, O., Gerard Spain, T., Ampe, C., 2018. Diurnal, synoptic and seasonal variability of atmospheric CO2 in the Paris megacity area. Atmos. Chem. Phys. 18, 3335–3362. https://doi.org/10.5194/acp-18-3335-2018.

Zhang, K., Gong, Y., Escobedo, F.J., Bracho, R., Zhang, X., Zhao, M., 2019. Measuring multi-scale urban forest carbon flux dynamics using an integrated eddy covariance technique. Sustain. (Switz.) 11. https://doi.org/10.3390/su11164335.

Zhao, C.L., Tans, P.P., 2006. Estimating uncertainty of the WMO mole fraction scale for carbon dioxide in air. J. Geophys. Res. Atmospheres 111, 1–10. https://doi.org/10.1029/2005JD006003.

Zhu, X.H., Lu, Peng, K.F., He, Z.R., Di, H., Xu, S.Q., 2022. Spatiotemporal variations of carbon dioxide (CO2) at Urban neighborhood scale: Characterization of distribution patterns and contributions of emission sources. Sustain. Cities Soc. 78, 103646 https://doi.org/10.1016/j.scs.2021.103646.